Evaluation of an Adaptive Unstructured Remeshing Technique for Integrated Fluid-Thermal-Structural Analysis

Pramote Dechaumphai*
NASA Langley Research Center, Hampton, Virginia 23665

An adaptive unstructured remeshing technique is evaluated for integrating fluid-thermal-structural analysis. The technique is combined with the finite element method to solve 1) the Navier-Stokes equations for high-speed compressible flow, 2) the energy equation for the structure's thermal response, and 3) the quasistatic equilibrium equations for the structural response. The remeshing technique and the analysis procedure are described. The effectiveness of the approach is evaluated with two application studies. The flow analysis of Mach 8 shock-shock interference on a 3-in.-diam cylinder is used as the first application to demonstrate the capability of the remeshing technique to capture the physics features of a complex high-speed flow. The applicability of the approach for the thermal and structural analyses of the structure is evaluated in the second application of a 0.25-in.-diam convectively cooled leading edge subjected to intense aerodynamic heating. The adaptive unstructured remeshing procedure and finite element solution algorithms combine to yield increased accuracy and efficiency over standard structured meshes.

Nomenclature

A = coolant passage area, Eq. (5), or finite element area, Eq. (8)
$[A^*]$ = Jacobian matrix
$[B]$ = viscous flux matrix
c = specific heat, Eq. (4), or material elastic constants, Eq. (12)
E, F = x and y flux components, respectively
H = load vector
h = convective heat transfer coefficient, Eq. (5), or element spacing parmeter, Eq. (16)
$[I]$ = identity matrix
$[K]$ = stiffness matrix
k = thermal conductivity
$[M]$ = mass matrix
$\dot{m}$ = coolant mass flow rate
$[N]$ = element interpolation function matrix
P = coolant passage perimeter
p = pressure
q = heat flux
$\{R\}$ = load vector
s = edge length of finite element
T = temperature
T_0 = reference temperature for zero stress
t = time
U = conservation variable
u, v = flow velocity components, Eq. (2), or displacement components, Eq. (13)
X, Y = principal coordinate directions
x, y = coordinate directions
Δt = time step
Δu = $u^{n+1} - u^n$
β = thermal expansion parameter
δ = boundary-layer thickness
ϵ = flow total energy, Eq. (2), or strain components, Eq. (12)
λ = eigenvalues
ϕ = key parameter for remeshing
ρ = density
$\sigma_x, \sigma_y, \tau_{xy}$ = fluid stress components, Eq. (2), or solid stress components, Eq. (7)

Subscripts

c = coolant
F = fluid
s = structural
T = thermal
1 = element internal flux
2 = flux across element boundary

Superscripts

I = inviscid
n = time step index, $t_n = n\Delta t$
T = transpose
V = viscous

Presented as Paper 90-0354 at the AIAA 28th Aerospace Sciences Meeting, Reno, NV, Jan. 8-11, 1990; received Feb. 13, 1990, revision received Sept. 14, 1990; accepted for publication Sept. 21, 1990. Copyright © 1991 by the American Institute of Aeronautics and Astronautics, Inc. No copyright is asserted in the United States under Title 17, U.S. Code. The U.S. Government has a royalty-free license to exercise all rights under the copyright claimed herein for Governmental purposes. All other rights are reserved by the copyright owner.

*Research Engineer, Cryogenic Fluids Technology Office. Member AIAA.

Introduction

DESIGN of lightweight structures and thermal protection systems for hypersonic vehicles depends on accurate prediction of aerothermal loads, structural temperatures and their gradients, as well as structural deformations and stresses. Adaptive unstructured remeshing techniques combined with the finite element method have been shown to improve significantly the efficiency and accuracy of the flow analysis. These benefits should also accrue for both thermal and structural analyses of structures. In addition, a universal remeshing procedure is needed for the development of an integrated fluid-thermal-structural analysis capability.

Research is currently underway to develop an integrated analysis approach[1] for accurately predicting each disciplinary behavior and their interactions. The approach uses the finite element method to solve 1) the Navier-Stokes equations for the aerodynamic flowfield and the aerothermal loads; 2) the structural energy equation for heat transfer and temperature distribution; and 3) the structural equations for deformation and stresses. For a complex aerodynamic flowfield, where a priori knowledge of the flow physics does not exist, an appropriate finite element mesh may not be constructed or even be designed easily. An adaptive mesh generation technique is required not only to construct and adapt the mesh automatically to represent the flowfield but also to minimize the number of unknowns and the analysis computational time. Thus, the current focus on the improvement of the integrated analy-

sis approach is to develop efficient adaptive unstructured mesh-generation techniques for each analysis discipline considered, including their interface requirements.

Adaptive mesh-generation techniques may be classified into two major categories: 1) refinement/derefinement, and 2) remeshing. The first category, the adaptive refinement/derefinement technique, can be further classified into three subcategories: a) the *h* method, b) the *p* method, and c) the *r* method. In the *h* method, the elements in the initial mesh are refined into smaller elements or derefined into larger elements.[2] The *p* method maintains the geometry of the elements of the initial mesh but increases (or decreases) the order of the polynomial used for the element interpolation function.[3] The *r* method keeps the number of elements and their connectivities the same but relocates the nodes.[4]

The remeshing technique, the second adaptive mesh-generation category, generates an entirely new mesh based on the solution obtained from an earlier mesh.[5] The technique combined with the finite element method has been applied successfully to several compressible flow problems with complex flow behavior.[6-8] The purpose of this paper is to extend the adaptive remeshing technique to both the thermal and structural analyses of structures. The adaptive remeshing technique will be evaluated to assess its effectiveness for the integrated fluid-thermal-structural analysis. The governing equations for the aerodynamic flow, structural heat transfer, and structural response will be introduced first. The analysis solution algorithms for solving these equations will be briefly described. The basic concepts of the adaptive remeshing technique will then be explained. Selection of indicators used for construction of new meshes for the three analysis disciplines will be discussed. Finally, the adaptive remeshing technique will be evaluated for 1) the fluid analysis of Mach 8 shock-shock interference on a 3-in.-diam cylinder where experimental data are available, and 2) the thermal-structural analysis of a 0.25-in.-diam convectively cooled leading edge subjected to intense aerodynamic heating simulating a Mach 16 flight condition. The issues of mesh continuity along the fluid/structure interface and between thermal and structural analyses for direct interdisciplinary data transfer will also be discussed.

Integrated Fluid-Thermal-Structural Procedure

Governing Equations

The equations for the aerodynamic flow, the structure heat transfer, and the structural response in two dimensions are briefly described herein.

Aerodynamic Flow

The equations for a laminar compressible flow are governed by the conservation of mass, momentum, and energy. These equations are written in conservation form as

$$\frac{\partial}{\partial t}\{U_F\} + \frac{\partial}{\partial x}\{E_F\} + \frac{\partial}{\partial y}\{F_F\} = 0 \tag{1}$$

where the subscript F denotes the fluid analysis. The conservation variables vector $\{U_F\}$ and the flux vectors in the x and y directions, $\{E_F\}$ and $\{F_F\}$, are given by

$$\{U_F\}^T = [\rho \quad \rho u \quad \rho v \quad \rho \epsilon] \tag{2a}$$

$$\{E_F\}^T = [E_F]^I + [E_F]^V$$

$$= [\rho u \quad \rho u^2 + p \quad \rho uv \quad \rho u\epsilon + pu]$$

$$- [0 \quad \sigma_x \quad \tau_{xy} \quad u\sigma_x + v\tau_{xy} - q_x] \tag{2b}$$

$$\{F_F\}^T = [F_F]^I + [F_F]^V$$

$$= [\rho v \quad \rho uv \quad \rho v^2 + p \quad \rho v\epsilon + pv]$$

$$- [0 \quad \tau_{xy} \quad \sigma_y \quad u\tau_{xy} + v\sigma_y - q_y] \tag{2c}$$

Superscripts I and V represent the inviscid and viscous flux vector components, respectively. The pressure p is related to the total energy assuming a calorically perfect gas (constant ratio of specific heats). The stresses σ_x, σ_y, and τ_{xy} are related to the velocity gradients by Stokes's law. The heat fluxes q_x and q_y are related to the temperature gradients by Fourier's law. The temperature-dependent viscosity is computed from Sutherland's law, and the thermal conductivity is computed assuming a constant Prandtl number of 0.72.

Structural Heat Transfer

The thermal response of the structure is governed by the energy equation written in conservation form as

$$\frac{\partial}{\partial t}(U_T) + \frac{\partial}{\partial x}(E_T) + \frac{\partial}{\partial y}(F_T) = H_T \tag{3}$$

where the subscript T denotes thermal analysis. For transient heat conduction, the conservation variable U_T and the heat flux components E_T and F_T are

$$dU_T = \rho_s c_s dT_s \tag{4a}$$

$$E_T = q_x = -k_s \partial T_s/\partial x \tag{4b}$$

$$F_T = q_y = -k_s \partial T_s/\partial y \tag{4c}$$

and H_T is the heat source. The structural heat flux components q_x and q_y are related to the temperature gradients by Fourier's law.

For a structure with internal convective cooling, the energy equation[9] for the coolant flow in a local x direction (flow direction) based on assumed uniform cross-sectional or bulk temperature T_c can also be written in the conservation form of Eq. (3) where

$$dU_T = \rho_c c_c dT_c \tag{5a}$$

$$E_T = (\dot{m} c_c T_c/A_c) - k_c \partial T_c/\partial x \tag{5b}$$

$$F_T = 0 \tag{5c}$$

$$H_T = hP(T_s - T_c) \tag{5d}$$

The flux E_T consists of the energy transport by convection (first term) and conduction (second term). The flux H_T represents the heat transfer between the structure and the coolant.

Structural Response

The structural response is governed by the quasistatic equilibrium equations assuming that the inertia effect is negligible. These equations are written in conservation form as

$$\frac{\partial}{\partial x}\{E_s\} + \frac{\partial}{\partial y}\{F_s\} = 0 \tag{6}$$

The flux vector components $\{E_s\}$ and $\{F_s\}$ are

$$\{E_s\}^T = [\sigma_x \quad \tau_{xy}] \tag{7a}$$

$$\{F_s\}^T = [\tau_{xy} \quad \sigma_y] \tag{7b}$$

where the stress components σ_x, σ_y, and τ_{xy} are related to the displacement gradients and the temperature by the generalized Hooke's law.

Analysis Solution Algorithms

An implicit/explicit upwind cell-centered algorithm[6] is used to solve the Navier-Stokes equations, Eqs. (1) and (2).[10] A flux-based Taylor-Galerkin finite element algorithm[8,11] is used to solve the thermal and structural equations, Eqs. (3-7). For

brevity, only essential features of the algorithms are highlighted herein.

Upwind Fluid Algorithm

The upwind cell-centered algorithm assumes a constant distribution of the conservation variables over an element. The inviscid flux $\{\bar{E}\}^I$ across element interface is determined by Roe's averaging procedure.[12] The viscous flux $\{\bar{E}\}^V$ across element interface is obtained by averaging the viscous fluxes computed at nodes that lie on the interface. Increments of the element conservation variables, $\Delta U = U^{n+1} - U^n$, are determined from

$$\left[[I]+\frac{\Delta t}{A}\sum_s\left([|A^*|]\frac{s}{2}-[B]\right)\right]\{\Delta U\} = -\frac{\Delta t}{A}\sum_s s\left[\{\bar{E}\}^I+\{\bar{E}\}^V\right] \tag{8}$$

where $[|A^*|]$ denotes a matrix whose entries are the absolute values of those in the Jacobian matrix $[A^*]$. The matrix $[B]$, which is associated with the viscous fluxes, accelerates the solution convergence in the viscous dominated regions. This fluid algorithm provides first order of accuracy $[\mathcal{O}(h)]$ in the inviscid flow dominated region, but the order of accuracy is close to 1.5 $[\mathcal{O}(h)^{1.5}]$ in the viscous flow dominated region.[10]

Flux-Based Taylor-Galerkin Algorithm

The flux-based Taylor-Galerkin algorithm assumes a linear distribution of the conservation variable U, as well as the flux components E and F over an element[1] in the form

$$U(x,y,t) = [N(x,y)]\{U(t)\} \tag{9a}$$

$$E(x,y,t) = [N(x,y)]\{E(t)\} \tag{9b}$$

$$F(x,y,t) = [N(x,y)]\{F(t)\} \tag{9c}$$

where $[N(x,y)]$ is a row matrix of finite element interpolation functions, and $\{E\}$ and $\{F\}$ are vectors of the element nodal flux quantities.

For the thermal analysis, the final finite element equations are in the form

$$[M]\{\Delta U_T\}^{n+1} = \{R_T\}_1^n + \{R_T\}_2^n \tag{10}$$

where $[M]$ is the mass matrix, and $\Delta U^{n+1} = U^{n+1} - U^n$ at time $n+1$. The two vectors on the right-hand side of Eq. (10) are associated with the fluxes within the element (subscript 1) and across the element boundary (subscript 2), respectively.

For the structural analysis, the final finite element equations are in the same form as the thermal equation, Eq. (10), but without the transient term:

$$\{R_S\}_1 + \{R_S\}_2 = 0 \tag{11}$$

By using the thermal stress-strain constitutive relations,

$$\sigma_i = c_{ij}\epsilon_j + \beta_i(T - T_0), \qquad i,j = 1,2,3 \tag{12}$$

and the strain-displacement relations, these nodal stress components associated with the $\{R_S\}_1$ vector can be written in terms of the nodal displacement components. Further algebraic manipulation of the finite element equation, Eq. (11), results in the standard form of

$$[K]\{U_S\} = \{R_S\}_2 + \{R_T\} \tag{13}$$

where $\{U_S\}$ consists of the unknowns of the nodal displacement components, $[K]$ is the element stiffness matrix, and $\{R_T\}$ is the thermal load vector. These matrices are evaluated in closed form and the details are given in Ref. 11.

Boundary Conditions

The fluid, thermal, and structural equations (1), (3), and (6) are solved subjected to appropriate boundary conditions. The boundary conditions for supersonic flow consist of specifying all conservation variables along the inflow surfaces. On the supersonic outflow surfaces, zero gradient of the conservation variables is imposed. A no-slip condition (velocities set to zero) is specified at the solid surface.

The boundary conditions for the thermal analysis are applied via the boundary vector $\{R_T\}_2$ shown in Eq. (10). The thermal boundary conditions may consist of 1) insulated boundary, 2) specified heating, 3) convection, and 4) radiation. For internal cooling, the convective boundary condition is applied for heat transfer between the structure and the coolant[9] [see Eq. (5)]. The boundary conditions for the structural analysis, such as the pressure load, are applied via the boundary vector $\{R_S\}_2$ shown in Eq. (13). The thermal load due to the change in the structure temperature is included in the structural equation via the vector $\{R_T\}$ shown in that equation.

Adaptive Remeshing Procedure

Remeshing Concept

The basic idea of adaptive remeshing is to construct a completely new mesh based on the solution obtained from the previous mesh. The new mesh will consist of clustered elements in regions with large solution gradients and few elements in the regions where the gradients are small. Element orientations are aligned with principal directions to provide the most accurate solution with a minimum number of elements. As an example, the shorter element side is in the direction normal to the shock line or through the boundary-layer thickness to capture large solution gradients. Based on these ideas, the adaptive remeshing technique consists of two steps: 1) the determination of the new element sizes and their orientations, and 2) the construction of the new mesh.

In the determination of the element size and orientation, the solid-mechanics concept of determining principal stresses and their directions from a given state of stress at a point is employed. For example, in the thermal analysis, small and clustered elements are needed in regions of large change in the temperature gradients. The temperature is thus considered as a key parameter to indicate where clustered elements are needed. At a typical node in the old mesh, the second derivatives[5,10] of the key parameter ϕ with respect to the global coordinates x and y are first computed:

$$\begin{bmatrix} \dfrac{\partial^2\phi}{\partial x^2} & \dfrac{\partial^2\phi}{\partial x\partial y} \\ \dfrac{\partial^2\phi}{\partial x\partial y} & \dfrac{\partial^2\phi}{\partial y^2} \end{bmatrix} \tag{14}$$

Then the eigenvalues λ, which represent the principal quantities in the principal directions X and Y where the cross derivatives vanish, are determined:

$$\lambda_1 = \left|\frac{\partial^2\phi}{\partial X^2}\right|, \qquad \lambda_2 = \left|\frac{\partial^2\phi}{\partial Y^2}\right| \tag{15}$$

These eigenvalues are the remeshing indicators and are used to determine the element spacings h_1 and h_2 in the two principal directions using the condition that

$$h_1^2\lambda_1 = h_2^2\lambda_2 = \text{const} \tag{16}$$

which result from distributing the finite element interpolation error equally, a condition for an optimal mesh.[13] This process

is performed for all of the nodes in the old mesh leading to the final condition of

$$h_1^2\lambda_1 = h_2^2\lambda_2 = \text{const} = h_{\min}^2\lambda_{\max} \tag{17}$$

Using this condition and specifying the required minimum element spacing $h_{\min}$, the new element spacings based on the solution of the old mesh are obtained and the new mesh is constructed.

Mesh construction is based on an advancing front technique.[5] Nodes are first placed along the domain boundary. Spacings between these nodes are dictated by the element spacing parameter h obtained earlier. At this stage, the front consists of a sequence of straight-line segments that connect consecutive boundary nodes, i.e., the domain boundary. Elements adjacent to the domain boundary are then constructed. The sizes and orientations of these elements are guided by the computed element spacing parameter h and the principal directions. As new elements are constructed from the domain boundary, the front is updated and represented by the new element sides. As the mesh construction goes on, the front changes its shape and propagates toward the domain interior. The generation process is terminated when the domain is filled completely with elements and the front vanishes.

Based on the condition shown in Eq. (17), the element size is generated according to the given minimum element spacing $h_{\min}$. Specifying too small a spacing $h_{\min}$ may result in a model with an excessive number of elements. On the other hand, specifying too large a spacing $h_{\min}$ may result in inadequate solution accuracy, or excessive analysis and remeshing cycles. These factors must be considered prior to generating a new mesh. Note that, because the technique generates an entirely new mesh with different nodal locations from the old mesh, interpolation of the solution from the old to the new mesh is necessary. The interpolated nodal quantities are used as the initial conditions for the new mesh to increase the analysis solution convergence.

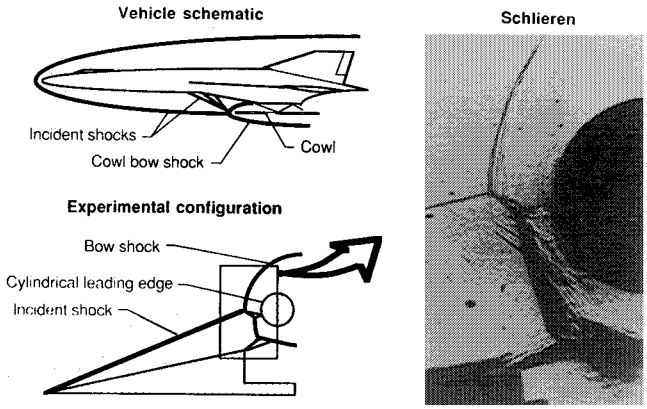

Fig. 1 Vehicle schematic, experimental configuration, and schlieren of type IV shock-shock interference.

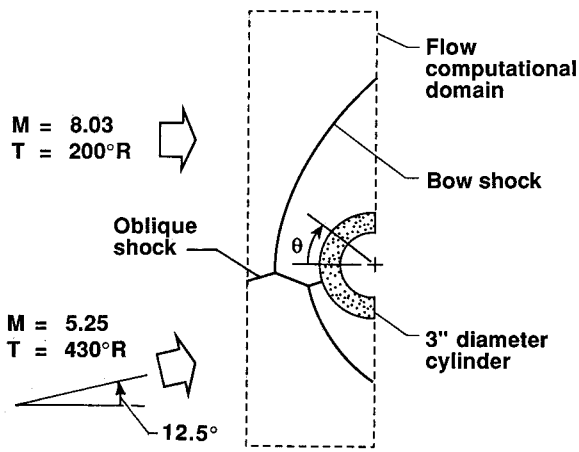

Fig. 2 Oblique and bow shock interaction pattern for Mach 8 shock-shock interference on a 3-in.-diam cylinder.

Fluid-Thermal-Structural Remeshing Parameters

The adaptive remeshing technique described requires a selection of proper key parameters [ϕ in Eq. (14)] for remeshing so that generated elements are properly sized, oriented, and clustered. Selection of the key parameters depends on the analysis discipline and its applications. In general, dependent variables are usually selected as the key parameters for remeshing. In the inviscid flowfield of high-speed compressible flow problems, the fluid density is normally selected as the key parameter[5,8] because density exhibits high gradients across shock and flow expansion waves. In viscous dominated flow regions, such as the boundary layer, other key parameters may be more appropriate. Key parameters of heating rate and skin friction may be used for more accurate analysis prediction of the aerothermal loads.[10]

For thermal problems, the temperature is selected as the key parameter so that the mesh generated can represent steep temperature gradients. For structural problems, stress is an appropriate choice for the key parameter so that regions with high stress concentration will be captured. However, the key parameter representing the stress should be a scalar quantity such as the Von Mises stress defined in two dimensions by

$$\sigma_{\text{Von Mises}} = \frac{1}{\sqrt{2}}\sqrt{(\sigma_x - \sigma_y)^2 + \sigma_x^2 + \sigma_y^2 + 6\tau_{xy}^2} \tag{18}$$

Note that the key parameter selected for remeshing may vary with applications. For problems that require accurate deformations rather than the stresses, an absolute displacement quantity may be preferred as the key parameter. The selection of these key parameters for remeshing in the three different analysis disciplines will be discussed in detail in the next section.

Evaluation of Integrated Analysis and Adaptive Remeshing Procedures

Two applications are presented to assess the adaptive unstructured remeshing procedures for integrated fluid-thermal-structural finite element analysis. The fluid analysis of Mach 8 shock-shock interference on a 3-in.-diam cylinder is used to illustrate the implementation of the adaptive remeshing technique for a complex flow and the interface requirements with the thermal and structural analyses of the structure. The remeshing technique for thermal and structural problems is demonstrated in the second application for a 0.25-in.-diam convectively cooled leading edge subjected to intense aerodynamic heating. All computations were made on the CRAY-2 and the VAX-8000 series computer systems.

Mach 8 Shock-Shock Interference on a Cylinder

Leading edges of hypersonic vehicles that experience intense stagnation-point pressures and heating rates are a significant challenge to the designer. For engine leading edges, such as the cowl shown in Fig. 1, intense aerothermal loads occur when the cowl bow shock is intersected by an oblique shock resulting in a supersonic jet that impinges on the leading-edge surface. The experimental configuration (lower left of Fig. 1), which simulates the vehicle forebody and cowl leading edge, was used to define the aerothermal loads.[14] The experimental configuration is rotated 180 deg relative to the vehicle. The schlieren photograph shows the supersonic jet interference pattern impinging on the surface of the cylinder. The interference pattern produces intense local amplification of the pressure and heat transfer rate in the vicinity of the jet impingement.

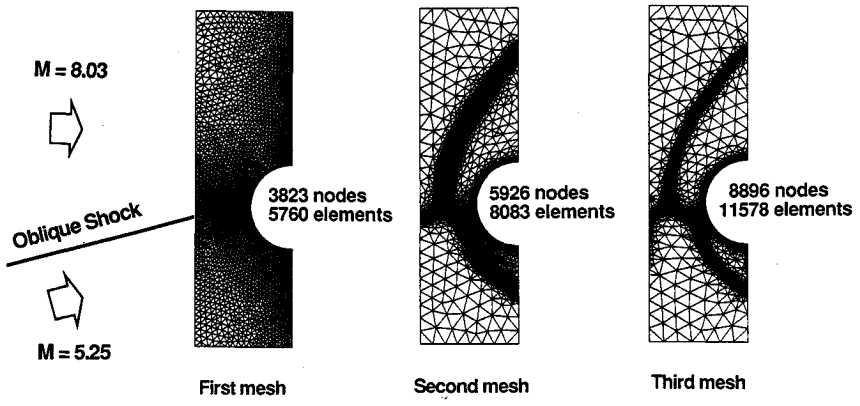

Fig. 3 Adaptive finite element mesh evolution of the flow domain for Mach 8 shock-shock interference on a 3-in.-diam cylinder.

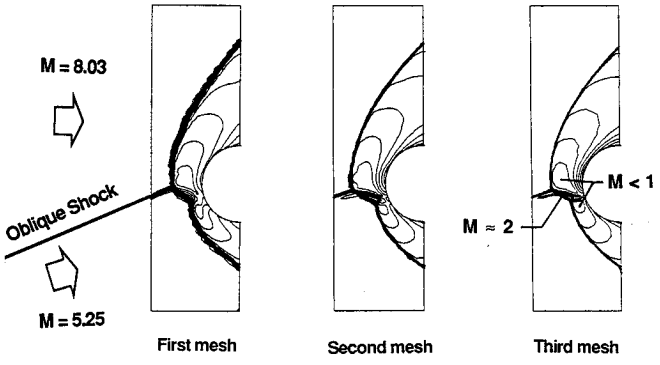

Fig. 4 Flow Mach number contours for the three adaptive unstructured finite element meshes for Mach 8 shock-shock interference on a 3-in.-diam cylinder.

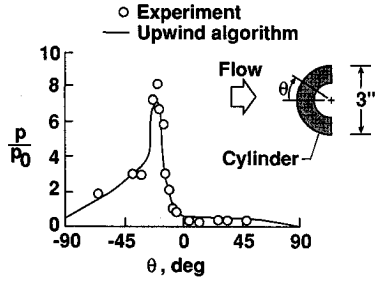

Fig. 5 Comparison of surface pressure distributions on a 3-in.-diam cylinder subjected to Mach 8 shock-shock interference.

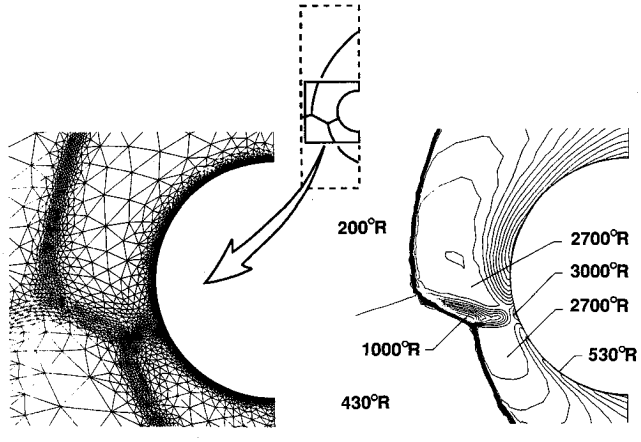

Fig. 6 Details of the finite element mesh and fluid temperature contours in the interaction region for Mach 8 shock-shock interference on a 3-in.-diam cylinder.

The flow-interaction pattern superimposed on the flow computational domain and the 3-in.-diam cylinder is shown schematically in Fig. 2. The inflow conditions above and below the oblique shock are shown in the figure. The supersonic jet impinges on the cylinder surface approximately 22 deg below the cylinder horizontal centerline. A first mesh shown in Fig. 3 is generated using a background mesh concept described in Ref. 5. A total of 4192 triangles are generated in the inviscid region and 1568 quadrilateral elements in the boundary layer. Quadrilateral elements are used in the boundary layer to capture steep temperature gradients for accurate aerodynamic heating-rate prediction. Details of the mesh in the boundary layer are given in Ref. 15. Using this first mesh, the fluid analysis is performed to obtain a flow solution as illustrated by the Mach number contours shown in Fig. 4. Based on this flow solution and the use of the fluid density as the key parameter for remeshing, the second mesh is created as shown in Fig. 3. The flow solution obtained from the first mesh is then interpolated and used as the initial condition for the second mesh. The same procedure is repeated on subsequent meshes until the converged flow solution is achieved (a total of three meshes in this case). The convergence criteria of the flow solution is given by the reduction of at least three orders of magnitude in the L^2 norm of the residuals of all of the conservation variables.

The Mach number contours shown in Fig. 4 demonstrate the improvement of the solution quality with the adaptive meshes. The Mach number distribution obtained from the third mesh shows improved sharpness of the shock interference pattern. The contours show a supersonic jet (Mach number ≈ 2) submerged within the subsonic regions between the bow shock and the cylinder. The supersonic flow in the jet terminates through a nearly normal shock prior to impinging on the cylinder surface. The predicted surface pressure distribution and the experimentally measured pressures [14] are normalized by the undisturbed stagnation pressure and are compared in Fig. 5. Good agreement between the predicted and experimental results are obtained for the pressure distribution, the peak pressure, and its locations.

Details of the finite element mesh and the flow temperature in the interaction region are shown in Fig. 6. The figure shows that elements are concentrated along the incident shock, the bow shock, and the supersonic jet to capture the steep flow gradients. The fluid temperature increases sharply across the bow shocks from a relatively low temperature (200 and 430°R) to approximately 2700°R. In the thin boundary layer, the temperature drops sharply to the cylinder temperature of 530°R resulting in high aerodynamic heating rates. The predicted surface heating rate normalized by the undisturbed stagnation heating rate is compared with the experimentally measured heating rate in Fig. 7. Although the predicted and experimental heating-rate distributions agree well, the peak predicted heating-rate amplification q/q_0 is only about 60% of that measured from the experiment. The lower predicted heating rate may be attributed to several sources including the

finite element mesh and the analysis algorithm. On the other hand, the higher experimental heating rate may be attributed to the freestream turbulence that is not taken into account in the analysis.

To generate an integrated fluid-thermal-structural finite element model, the use of common nodes along the fluid/structure interface is preferred[16] as highlighted in Fig. 8. Several adaptive meshing techniques are feasible for the thermal-structural analysis of the structure which include the mesh refinement/derefinement technique and the remeshing technique developed for the flow problems. Before selecting one of these techniques, their effectiveness for thermal and structural problems must be evaluated. An initial evaluation of the adaptive remeshing technique for both the thermal and structural analyses is performed in the next application.

Convectively Cooled Leading Edge

A 0.25-in.-diam convectively cooled leading edge subjected to intense aerodynamic heating is used to evaluate the adaptive remeshing technique for both the thermal and structural analyses and to identify requirements for the remeshing parameters for thermal stress problems. The example problem represents a hypersonic vehicle operating at Mach 16 which causes the vehicle nose bow shock to intersect with the cowl leading-edge bow shock. The intersection produces the type IV supersonic jet interference pattern similar to that described in the first application. Because of the smaller leading-edge diameter and the higher Mach number conditions, the heating rate is very intense with a peak of nearly 30,000 Btu/ft^2-s (see Ref. 1).

The leading-edge geometry and boundary conditions are shown schematically in Fig. 9. The outer surface is subjected to the aerodynamic heating and emits radiant energy to space. The inner surface is convectively cooled by the direct impingement of a sonic hydrogen jet stream with an inlet temperature of 50°R. The 1350 quadrilateral element mesh shown in Fig. 10a is typical of a structured mesh. The mesh has been used previously[1] for predicting transient thermal-structural response of the leading edge as the vehicle nose bow shock sweeps across the cowl during the vehicle acceleration. The mesh is graded in the radial direction but is uniform in the circumferential direction. The leading-edge material is assumed to be copper because of its high thermal conductivity.[1] The predicted steady-state leading-edge temperature contours are shown in Fig. 10b. The peak temperature of 766°R is at the jet impingement location where the heating rate is a maximum. In spite of the high thermal conductivity of the material, the temperature gradients are also high in this region. The problem is, therefore, suitable to be used for evaluating the adaptive remeshing technique for the thermal analysis of the structure.

The same adaptive remeshing procedure described for the flow problem is applied for the thermal analysis of the leading edge. A fairly uniform mesh consisting of 885 triangles, shown in Fig. 11a, is first constructed and the thermal analysis is performed to obtain the temperature distribution. Then the adaptive mesh shown in Fig. 11b is generated using the temperature as the key parameter for remeshing to provide clustered elements in the region with high temperature gradients. The temperature distribution obtained from the second mesh is almost identical (a difference of 0.2%) to that obtained from the nonadaptive mesh shown in Fig. 10b. However, the number of unknowns required for the adaptive unstructured mesh is only 27% of those used in the structured mesh. The reduction of the number of unknowns (and elements) results in less computer storage requirement. In addition, the computational time required by the adaptive unstructured mesh is only 31% of that needed by the structured mesh. Note also that, as shown in Fig. 11b, several elements are required through the thickness where the peak heating occurs and only one or two elements are required near the end of the leading edge. Hence, only an unstructured mesh technique would optimize the mesh.

To evaluate the effectiveness of the adaptive remeshing technique to represent both the thermal and mechanical stress fields, structural boundary constraints at the upper and lower leading-edge sections are introduced. The inner surface nodes at the constraint are fixed ($u = v = 0$, see Fig. 12a) to simulate the constraints caused by the internal fins that support the leading edge from the inner primary structure. To highlight

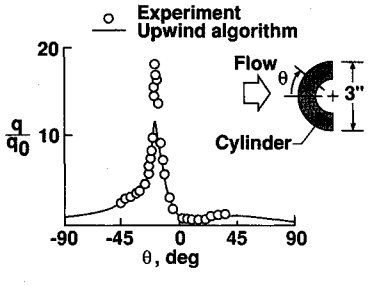

Fig. 7 Comparison of surface heating-rate distributions on a 3-in.-diam cylinder subjected to Mach 8 shock-shock interference.

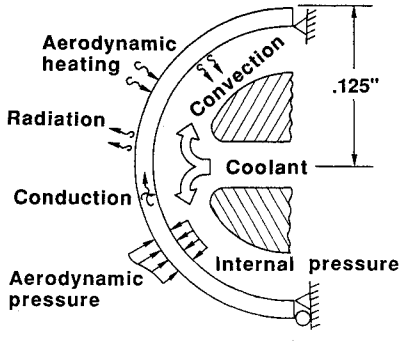

Fig. 9 Schematic thermal-structural analysis model of 0.25-in.-diam leading edge with boundary conditions.

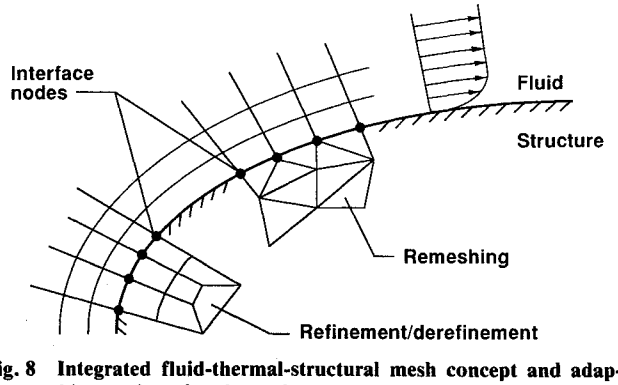

Fig. 8 Integrated fluid-thermal-structural mesh concept and adaptive meshing options for thermal-structural analysis of the structure.

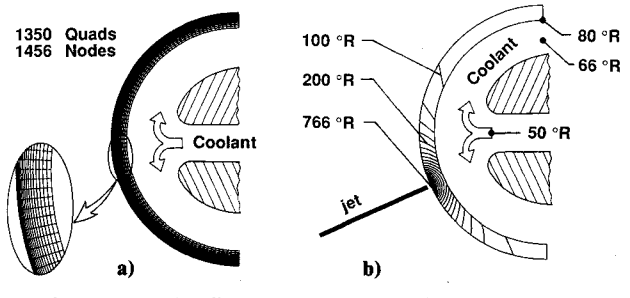

Fig. 10 Nonadaptive finite element mesh and temperature contours for convectively cooled leading edge: a) nonadaptive structured mesh, and b) temperature contours.

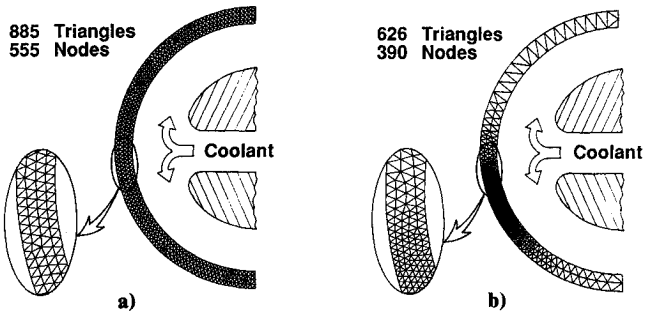

Fig. 11 Adaptive finite element mesh evolution for thermal analysis of convectively cooled leading edge: a) first mesh, and b) second mesh.

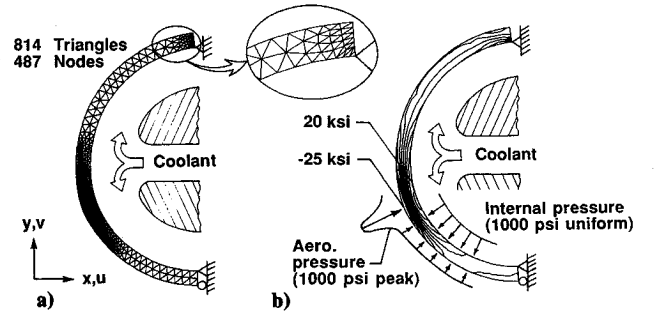

Fig. 12 Final adaptive solution for convectively cooled leading edge subjected to thermal and pressure loads using indicators of temperature and Von Mises stress simultaneously: a) adaptive mesh, and b) circumferential stress.

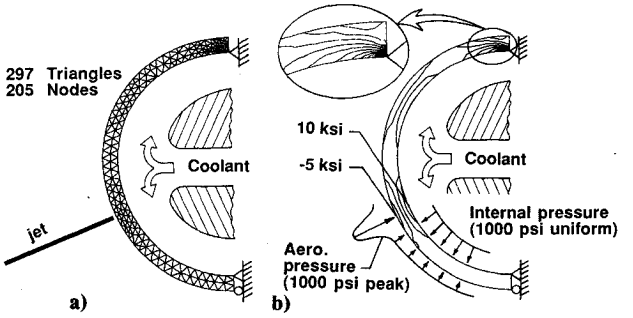

Fig. 13 Final adaptive solution for convectively cooled leading edge subjected to pressure load using indicator of Von Mises stress: a) adaptive mesh, and b) circumferential stress.

the remeshing capability for generating clustered elements in the regions needed, the rest of the nodes on both sections are constrained differently. These nodes are free to move on the upper section but are constrained in the horizontal direction on the lower section. In addition to the thermal loads, the leading edge is also subjected to mechanical loads from 1) the aerodynamic pressure that has a distribution similar to that shown in Fig. 5 but with a peak pressure of 1000 psia, and 2) the uniform internal coolant pressure of 1000 psia.

The adaptive thermal mesh shown in Fig. 11b is used as the initial mesh for the structural analysis. The same analysis procedure is applied by first obtaining the structural analysis solution and then remeshing. In the remeshing process, nodal temperatures of the new mesh are interpolated from the nodal temperatures of the thermal mesh shown in Fig. 11b. For thermal stress problems, high stresses normally occur in regions of high temperature gradients. High stress concentrations may also occur at corners or supports even though the temperature is uniform. Thus, to represent both the thermal stress and the stress concentration, key parameters for remeshing based on the temperature and the Von Mises stress are used simultaneously. Each key parameter identifies an element size for equal distribution of finite element interpolation error [see Eq. (17)], however, the minimum element size is always selected. A new adaptive mesh generated by using these two remeshing parameters is shown in Fig. 12a. Elements are clustered near the jet impingement location for modeling high thermal stresses from the high temperature gradients, and at the region near the upper support where the stress concentration occurs. The corresponding structural response, based on a linear elastic behavior assumption, is shown by the circumferential stress contours superimposed on the deformed leading edge in Fig. 12b. The figure shows that a peak compressive stress of 25 ksi occurs at the jet impingement location and a high stress concentration occurs near the singular point at the upper support.

Superposition of the solutions from different load cases is a popular technique in the structural analysis; hence, the effect of adaptive unstructured remeshing on superpositioning is investigated. Since the thermal mesh is probably adequate for the thermal stress analysis, the adaptive remeshing technique for the structural analysis is further evaluated for the case in which the thermal load is not present. The leading edge is subjected only to mechanical loads that consist of the external aerodynamic pressure and the internal coolant pressure. The Von Mises stress is used as the remeshing parameter, and the adaptive mesh generated is shown in Fig. 13a. Similar to the previous case, clustered elements are in the region near the upper support where the stress concentration occurs. The corresponding predicted structural response of the circumferential stress contours is shown in Fig. 13b. The predicted compressive stress of 5 ksi at the jet impingement location is much lower than the stress that occurred for the case with the thermal load. Obviously, superposition of the results for separate mechanical and thermal stress analyses would require interpolation of the results. Hence, the adaptive remeshing and analysis should be used for the combined load case.

As mentioned earlier, the use of common nodes along the fluid/structure interface is preferred for integrating fluid-thermal-structural finite element model (see Fig. 8). The approach not only permits direct data transfer between the different analysis disciplines but also provides consistency for the analysis formulation. As an example of a coupled fluid/thermal problem, the interface nodal temperatures can be obtained by solving the coupled energy equation of the flow and the structure[1] with the requirements that at the interface 1) the temperatures of the fluid and the structure are identical, and 2) the heat flux is continuous. For some problems, the requirement of common fluid/structure interface nodes to preserve the mesh continuity may result in an excessive number of nodes in one of the disciplines. For example, a high stress concentration may occur near the fluid/structure interface that may require a large number of structural nodes even though the flow near that region is simple. In addition, evaluation of other adaptive meshing techniques (such as refinement/derefinement technique) for the thermal-structural analysis of the structure is also needed.

For coupled fluid-thermal-structural analysis, both the thermal and structural response of the structure can affect the flowfield. The flowfield has to be updated to include the effects of 1) the change of the structure's surface temperature, and 2) the structural deformation. The structure may deform into or away from the initial flowfield, and updating the flow computational domain is necessary. The new flowfield may govern regions previously occupied by the structure where the flow information does not exist. These are some of the future issues that will be encountered and have to be clarified prior to applying the adaptive remeshing technique to coupled interdisciplinary problems.

Concluding Remarks

An adaptive unstructured remeshing technique was evaluated for integrated fluid-thermal-structural analysis. The tech-

nique generates an entirely new mesh based on the solution obtained from a previous mesh. The new mesh consists of clustered elements in the regions with high solution gradients and few elements in the regions where the gradients are small. The capability of the remeshing technique was demonstrated for the fluid, thermal, and structural analyses. The finite element formulations used for the three disciplines were presented. The basic idea behind the remeshing technique was described, and the remeshing indicators and requirements were identified.

Two applications were presented to assess the effectiveness of the remeshing technique. The fluid analysis of Mach 8 shock-shock interference on a 3-in.-diam cylinder was presented as the first application to demonstrate the benefit of the remeshing technique for complex flow. Fluid density was used as the key parameter for remeshing. The remeshing technique was extended to the thermal and structural analyses of the structure. The applicability of the technique to thermal stress problems was demonstrated with a 0.25-in.-diam convectively cooled leading edge subjected to intense aerodynamic heating. Temperature was selected as the key parameter for remeshing in the thermal analysis so that clustered elements are generated in regions of high temperature gradients. The technique provides the same temperature solution accuracy compared to a refined structured mesh but with a significant reduction in the number of unknowns and computational time. For the structural analysis of the leading edge subjected to both thermal and pressure loads, remeshing parameters of the temperature and the Von Mises stress are used simultaneously to provide clustered elements in regions of high thermal and mechanical stresses as well as regions with a stress concentration. The mesh is for the combined thermal and mechanical load cases to avoid the superposition of the solutions from each separate load case which would decrease the solution accuracy.

The applications have demonstrated the viability of the adaptive unstructured remeshing finite element method to provide efficient accurate solutions for complex flow-thermal-structural behavior.

References

[1]Dechaumphai, P., Thornton, E. A., and Wieting, A. R., "Flow-Thermal-Structural Study of Aerodynamically Heated Leading Edges," *Journal of Spacecraft and Rockets,* Vol. 26, No. 4, 1989, pp. 201-209.

[2]Ramakrishnan, R., Bey, K. S., and Thornton, E. A., "Adaptive Quadrilateral and Triangular Finite-Element Scheme for Compressible Flows," *AIAA Journal,* Vol. 28, No. 1, 1990, pp. 51-59.

[3]Dechaumphai, P., and Thornton, E. A., "Nodeless Variable Finite Elements for Improved Thermal-Structural Analysis," *Proceedings of the International Conference on Finite-Element Methods,* Gordon and Breach Science Publishers, New York, Aug. 1982, pp. 139-144.

[4]Lohner, R., Morgan, K., and Zienkiewicz, O. C., "Adaptive Grid Refinement for Compressible Euler and Navier-Stokes Equations," *Proceedings of the International Conference on Accuracy Estimates and Adaptive Refinements in Finite-Element Computations,* Vol. 2, Wiley, New York, 1984, pp. 189-202.

[5]Peraire, J., Vahjdati, M., Morgan, K., and Zienkiewicz, O. C., "Adaptive Remeshing for Compressible Flow Computations," *Journal of Computational Physics,* Vol. 72, 1987, pp. 449-466.

[6]Thareja, R. R., Stewart, J. R., Hassan, O., Morgan, K., and Peraire, J., "A Point Implicit Unstructured Grid Solver for the Euler and Navier-Stokes Equations," *International Journal for Numerical Methods in Fluids,* Vol. 9, 1989, pp. 405-425.

[7]Dechaumphai, P., and Wieting, A. R., "Coupled Fluid-Thermal-Structural Analysis for Aerodynamically Heated Structures," *Finite Element Analysis in Fluids,* edited by T. J. Chung and G. R. Karr, Univ. of Alabama in Huntsville Press, Huntsville, AL, April 1989, pp. 165-171.

[8]Dechaumphai, P., Weiting, A. R., and Pandey, A. K., "Fluid-Thermal-Structural Interaction of Aerodynamically Heated Leading Edges," AIAA Paper 89-1227, April 1989.

[9]Thornton, E. A., and Wieting, A. R., "Finite-Element Methodology for Transient Conduction/Forced Convection Thermal Analysis," *Heat Transfer, Thermal Control, and Heat Pipes,* edited by Walter B. Olstad, Vol. 70, Progress in Astronautics and Aeronautics, AIAA, New York, 1980, pp. 77-103.

[10]Vemaganti, G. R., "An Adaptive Remeshing Finite-Element Method for High-Speed Compressible Flows Using Quadrilateral and Triangular Elements," Ph.D. Dissertation, Old Dominion Univ., Norfolk, VA, May 1989.

[11]Pandey, A. K., Dechaumphai, P., and Wieting, A. R., "Thermal-Structural Finite-Element Analysis Using Linear Flux Formulation," AIAA Paper 89-1224, April 1989.

[12]Gnoffo, P. A., "Application of Program LAURA to Three-Dimensional AOTV Flowfields," AIAA Paper 86-0565, Jan. 1986.

[13]Oden, J. T., and Carey, G. F., *Finite Elements: Mathematical Aspects,* Prentice-Hall, Englewood Cliffs, NJ, 1981.

[14]Wieting, A. R., and Holden, M. S., "Experimental Shock-Wave Interference Heating on a Cylinder at Mach 6 and 8," *AIAA Journal,* Vol. 27, No. 11, 1989, pp. 1557-1565.

[15]Dechaumphai, P., "Evaluation of an Adaptive Unstructured Remeshing Technique for Integrated Fluid-Thermal-Structural Analysis," AIAA Paper 90-0556, Jan. 1990.

[16]Thornton, E. A., and Dechaumphai, P., "Coupled Flow, Thermal, and Structural Analyses of Aerodynamically Heated Panels," *Journal of Aircraft,* Vol. 25, No. 11, 1988, pp. 1052-1059.